Optical instabilities in a three-level Λ and V system inside a double cavity

H. Aswath Babu and Harshawardhan Wanare
Department of Physics, Indian Institute of Technology Kanpur, Kanpur 208016, India
(Received 1 February 2013; published 9 August 2013)

We obtain optical instabilities in all-optical bistable systems arising from competing cooperative pathways at low input light levels. In particular, for three-level atomic systems in the Λ and V configuration interacting with two independent cavity modes, we identify the necessary conditions related to the incoherent pathways required to obtain instabilities. The instabilities arise when atomic states involved in the bistable transition are *leaky* and have substantial population, where the incoherent processes directly hinder the cooperative preparation of the atomic ensemble.

DOI: 10.1103/PhysRevA.88.023814 PACS number(s): 42.65.Pc, 42.65.Sf, 42.50.Gy

I. INTRODUCTION

Optical instabilities in atom-cavity coupled systems have been widely studied, particularly in the context of lasers and optical bistability [1–5]. The phenomenon of all-optical bistability (AOB) is a cornerstone effect arising from cooperative atom-field dynamics. This phenomenon has been extensively studied in order to realize all-optical switching, as well as nonlinear dynamical effects such as self-pulsing and chaos [6,7]. We focus our attention on optical instabilities in AOB systems, particularly at low-light levels. Traditionally, the occurrence of optical instabilities arises in two well-known regimes: one involves the atom coupling to multiple longitudinal modes of the cavity and the other involves a single-cavity mode coupled to the atom and the instability occurs in the upper branch (also known as one-atom branch) of AOB [6–8], where the cooperative effect is nonexistent. The former class of instabilities, arising from large number of modes, results from an interplay of a variety of time scales leading to chaos and self-pulsing. The latter effect involves an intense intracavity field that saturates the collection of atoms in absorptive AOB along with optical pumping, and thus does not involve any cooperative effects. In an effort to realize controllable optical instabilities in AOB in the regime where cooperative effects play a central role, we propose coupling two adjacent transitions in a multilevel atom to bichromatic fields which experience independent feedback, leading to competing cooperative behavior and the resulting optical instabilities. In our previous work, we have shown the existence of instabilities and negative hysteresis in a three-level ladder (Ξ) system with such double-feedback AOB [9,10].

Earlier, a three-level atom in the Λ-type configuration operated under an electromagnetic induced transparency (EIT) regime was exploited to obtain instabilities using single-cavity feedback [11]. Recently, controlled optical switching using a double cavity having a K-type multilevel system was proposed [12]. We seek to determine if instabilities can be obtained universally in every few-level atomic configuration. It appears that the nature of the incoherent process plays a central role in the cooperative regime. So far, the three-level atom in the V- and Λ-type configurations has not been explored in the context of double-feedback AOB to observe optical instabilities. However, the three-level V-system AOB has been studied in the context of spontaneous-emission-induced quantum interference, leading to variation in the AOB switching thresholds [13] as well as multistability [14]. In the absence of such quantum interference, the V system exhibits regular switching devoid of any optical instability [15,16]. In this paper, we study both the Λ and V system in double-cavity AOB and are able to pin down the precise nature of the decay processes that could lead to controlled optical instabilities such as self-pulsing and chaotic output at low-light levels in the cooperative branch. Such instabilities can be obtained in conventional optical switches by providing an extra coupling, for applications in secure communications [17] and synchronization of chaos [18].

The organization of the paper is as follows. In the next section, we describe the necessary theoretical model, which is followed by results and discussion associated with the Λ and V system, respectively. We conclude in the last section.

II. THEORETICAL MODEL

The schematic in Fig. 1 indicates the three-level Λ and V configurations and the setup involving the double-cavity feedback, wherein two optical fields simultaneously interact with the atomic medium. We present the density matrix equations that govern the evolution of the atoms accompanied by the field equations that capture feedback in the slowly varying envelope approximation [19]. We confine ourselves to the mean-field approximation, widely used in the context of AOB, thus ignoring any spatial dependence of the field within the cavity. The propagation of the two fields inside the active medium (atomic vapor) are chosen to be copropagating in order to eliminate the first-order Doppler effect and the associated broadening [20].

The two coherent fields having amplitude E_1 and E_2 at frequencies ω_1 and ω_2 couple to the atom in the Λ configuration along the transitions $|2\rangle \leftrightarrow |1\rangle$ and $|2\rangle \leftrightarrow |3\rangle$, respectively, and are shown in Fig. 1(a). The density matrix equations are obtained under the rotating-wave approximation and are given as

$$\frac{\partial \rho_{11}}{\partial t} = 2\gamma_1 \rho_{22} - 2\nu \rho_{11} + iG_1 \rho_{21} - iG_1^* \rho_{12},$$

$$\frac{\partial \rho_{12}}{\partial t} = -(\gamma_1 + \gamma_2 + \nu - i\Delta_1)\rho_{12} - iG_1(\rho_{11} - \rho_{22}) - iG_2^* \rho_{13},$$

$$\frac{\partial \rho_{13}}{\partial t} = -[\nu + i(\Delta_1 - \Delta_2)]\rho_{13} + iG_1 \rho_{23} - iG_2 \rho_{12},$$

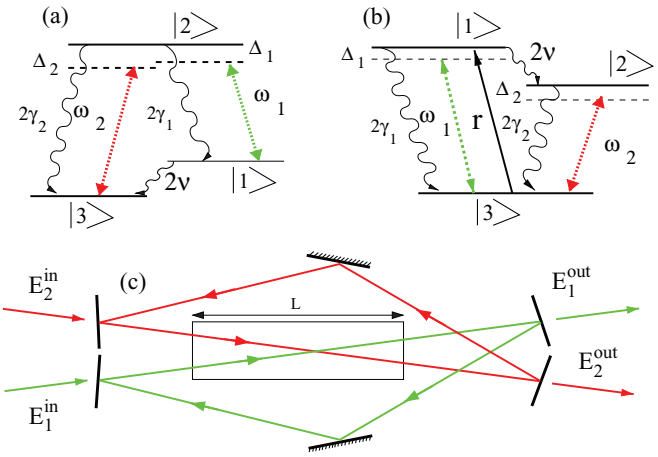

FIG. 1. (Color online) (a), (b) Schematic of three-level atom in Λ and V configuration interacting with the two coherent fields having amplitudes E_1 and E_2 at frequencies ω_1 and ω_2, respectively. In the case of a V system, the solid arrow from level $|3\rangle$ to $|1\rangle$ indicates incoherent pumping of rate r. (c) Two independent unidirectional ring cavities where the active medium contained within the length L interacts simultaneously with the two fields.

$$\begin{aligned}
\frac{\partial\rho_{22}}{\partial t} &= -2(\gamma_1+\gamma_2)\rho_{22} + iG_1^*\rho_{12} - iG_1\rho_{21} \\
&\quad + iG_2\rho_{32} - iG_2^*\rho_{23}, \\
\frac{\partial\rho_{23}}{\partial t} &= -(\gamma_1+\gamma_2+i\Delta_2)\rho_{23} + iG_1^*\rho_{13} - iG_2(\rho_{22}-\rho_{33}), \\
\frac{\partial\rho_{33}}{\partial t} &= 2\nu\rho_{11} + 2\gamma_2\rho_{22} + iG_2^*\rho_{23} - iG_2\rho_{32}, \qquad (1)
\end{aligned}$$

where $\Delta_1 = \omega_{21} - \omega_1$ and $\Delta_2 = \omega_{23} - \omega_2$ are the atomic detunings, $G_1 = \vec{d}_{21}\cdot\vec{E}_1/\hbar$, $G_2 = \vec{d}_{23}\cdot\vec{E}_2/\hbar$ are the Rabi frequencies, and $2\gamma_1$ and $2\gamma_2$ are the spontaneous-emission decay rates from the levels $|2\rangle\rightarrow|1\rangle$ and $|2\rangle\rightarrow|3\rangle$, respectively. The ground-state decoherence arising from the nonradiative decay associated with the transition $|1\rangle \leftrightarrow |3\rangle$ is described by the decay rate 2ν.

The three-level atoms in the V configuration couple to two fields having amplitude E_1, E_2 at frequencies ω_1, ω_2 along the transitions $|1\rangle \leftrightarrow |3\rangle$ and $|2\rangle \leftrightarrow |3\rangle$, respectively, which is shown in Fig. 1(b). The density matrix equations in the rotating-wave approximation are given as

$$\begin{aligned}
\frac{\partial\rho_{11}}{\partial t} &= -2\gamma_1\rho_{11} - 2\nu\rho_{22} + r\rho_{33} + iG_1\rho_{31} - iG_1^*\rho_{13}, \\
\frac{\partial\rho_{12}}{\partial t} &= -[\gamma_1+\gamma_2+\nu+i(\Delta_1-\Delta_2)]\rho_{12} + iG_1\rho_{32} \\
&\quad - iG_2^*\rho_{13}, \\
\frac{\partial\rho_{13}}{\partial t} &= -(\nu+\gamma_1+i\Delta_2)\rho_{13} - iG_2\rho_{12} - iG_1(\rho_{11}-\rho_{33}), \\
\frac{\partial\rho_{22}}{\partial t} &= -2\gamma_2\rho_{22} + 2\nu\rho_{11} - iG_2^*\rho_{23} + iG_2\rho_{32}, \\
\frac{\partial\rho_{23}}{\partial t} &= -(\gamma_2+i\Delta_2)\rho_{23} - iG_2(\rho_{22}-\rho_{33}) - iG_1\rho_{21}, \\
\frac{\partial\rho_{33}}{\partial t} &= 2\gamma_1\rho_{11} + 2\gamma_2\rho_{22} - r\rho_{33} + iG_2^*\rho_{23} - iG_2\rho_{32} \\
&\quad + iG_1^*\rho_{13} - iG_1\rho_{31}, \qquad (2)
\end{aligned}$$

where $\Delta_1 = \omega_{13} - \omega_1$ and $\Delta_2 = \omega_{23} - \omega_2$ are the atomic detunings, $G_1 = \vec{d}_{13}\cdot\vec{E}_1/\hbar$, $G_2 = \vec{d}_{23}\cdot\vec{E}_2/\hbar$ are the Rabi frequencies, and $2\gamma_1$ and $2\gamma_2$ are the spontaneous-emission rates from the levels $|1\rangle \rightarrow |3\rangle$ and $|2\rangle \rightarrow |3\rangle$, respectively. Excited-state decoherence resulting from a nonradiative decay pathway from $|1\rangle$ to $|2\rangle$ is indicated with a decay rate 2ν. An incoherent pump applied to transfer atomic population from level $|3\rangle$ to $|1\rangle$ plays an important role in the nonlinear dynamical behavior of the V system, whose strength is described with rate r [21].

Here, the optical fields having amplitudes E_1 and E_2 circulate within two independent ring cavities, which provide sufficient feedback that leads to cooperative phenomena. The equations of motion of the fields consisting of information of boundary conditions as well as cavity feedback associated with the individual cavities are given as follows:

$$\frac{\partial x_i}{\partial t} = \kappa_i\left[-x_i(1+i\theta_i) + y_i + 2iC_i\rho_{mn}\right], \qquad (3)$$

where the index "i" refers to the fields 1 and 2 at frequencies ω_1 and ω_2, respectively, and which involves normalized input fields $y_i = \vec{d}_{mn}\cdot\vec{E}_i^{\rm in}/\hbar\gamma_i\sqrt{T_i}$ and output fields $x_i = \vec{d}_{mn}\cdot\vec{E}_i^{\rm out}/\hbar\gamma_i\sqrt{T_i}$, where $\vec{E}_i^{\rm in(out)}$ is the amplitude of the input (output) field associated with the $i^{\rm th}$ field that couples to the transition $|m\rangle \leftrightarrow |n\rangle$ whose dipole moment is $\vec{d}_{mn}$. The subscripts m and n denote the appropriate transition involving the atomic levels $|1\rangle$, $|2\rangle$, and $|3\rangle$, as shown in Figs. 1(a) and 1(b). The other terms in the above equation are the cavity decay $\kappa_i = cT_i/\mathcal{L}_i$, the scaled cavity detuning $\theta_i = \delta_i^c/T_i$, and the cooperative parameter $C_i = \alpha_i L/2T_i$, where $\delta_i^c = (\omega_i^c - \omega_i)\mathcal{L}/c$ is the normalized cavity detuning, L is the extent of the region which contains the active atoms, α_i is the absorption coefficient associated with field at frequency ω_i, $\mathcal{L}_i$ is the total length of the corresponding cavity whose resonant frequency is ω_i^c, and the transmission coefficient of the input and output mirrors is T_i. All the frequency units are normalized with respect to the spontaneous decay rate γ_2, unless specified otherwise. The derivation of the above equations and the details of the numerical techniques are along the lines discussed extensively in Ref. [10].

We have self-consistently solved the above set of nonlinear atom and field equations in the steady state. We have undertaken a linear stability analysis, which allows us to map out the various regions of stability such as those involving stable switching, self-pulsing, or chaotic output. The bifurcation diagram is also obtained in order to understand the various nonlinear dynamical features exhibited in these AOB double-cavity systems.

III. RESULTS AND DISCUSSION

The double-cavity AOB system interacting with three-level atoms exhibits a variety of nonlinear dynamical effects which seem to occur in all three types of atomic configurations (Λ, V, and Ξ systems) in appropriate regimes. It is such comparative analysis that provides insight into the optical instability and its dependence on decay channels. Earlier studies with three-level atoms have adopted a simplified approach wherein the intermediate level is adiabatically eliminated [22,23] and the effective interaction encompasses the two-photon transition

without taking into account the effects of the intermediate state. This assumption effectively rules out any optical instability [24,25]. Such simplified treatment leads to normal stable switching. In this paper, we focus our attention on nonlinear dynamical effects associated with the cooperative (lower) branch of AOB in the Λ and V atoms, which have not been presented earlier [9,10]. Our earlier study of the Ξ system in the double cavity exhibits AOB, and we found that the variation in the ratio of the cooperative parameter along the two adjacent transitions and the variation of the decays results in behaviors such as self-pulsing, chaos, and negative hysteresis. However, the Λ and V system are quite distinct in their behavior with regard to double-cavity AOB.

It is important to bring out the difference between the instabilities presented here and the single-mode instabilities that arise in the upper branch under strong-field conditions, which are known to be well understood in the literature [6–8]. The conventional upper-branch instability invariably results from an intense nonlinear atom-field interaction and a phase-mismatched feedback arising from nonzero cavity detuning. The fast nonlinear response and slow optical pumping are known to be the two competing time scales that result in self-pulsing. In contrast, our double-cavity instabilities arise in the lower cooperative branch of AOB without involving finite cavity detuning. The cooperative branch, which intrinsically involves different physical processes, is responsible for the instability.

In the case of the single-feedback AOB system having a multilevel atomic medium, the instability associated with the cooperative branch arises from the *leaky* population of the lower atomic level involved in the AOB transition [26]. The preparation of the atoms in the lower state such that they exhibit cooperative (or *collective*) phenomena is necessary to observe normal switching. A leakage of atomic population from such a coherently prepared lower atomic level leads to instability. Such an effect is easily realized in the three-level ladder system with AOB along the upper transition. The leakage of population occurs via spontaneous emission into the ground state, leading to the instability in the lower cooperative branch. Such an arrangement can also occur in the Λ system wherein incoherent decay coupling the pair of ground states is essential to obtain instability in the cooperative branch. This situation cannot arise in a V system, as the AOB field directly couples to the ground state. Hence, a V system does not exhibit instability in the lower cooperative branch.

The various incoherent decay processes, including spontaneous emission, relaxation of the ground-state coherence, as well as any incoherent pumping pathways to and from different atomic states, play a critical role in dictating the nonlinear dynamical behavior of the double-cavity AOB system. Before taking the discussion further, we recall some of the important results reported in our previous work [9,10], which are pertinent in developing our understanding of the current system. The three-level Ξ system is coupled to a pair of coherent fields that simultaneously experience feedback in two independent ring cavities, apart from normal stable switching, where the cavity fields exhibit either periodic self-pulsing or chaotic nonlinear dynamical behavior in the cooperative branch. The system exhibits a period doubling route to chaos. Another interesting effect is the presence of negative hysteresis at low-light levels, whereas the conventional (positive) hysteresis continues to occur at higher incident intensities.

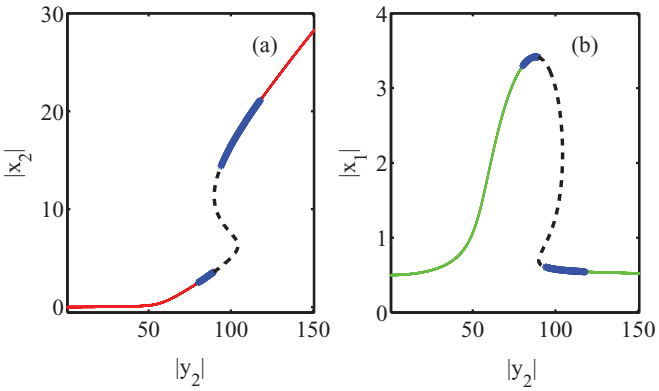

FIG. 2. (Color online) Λ system. (a), (b) Bistable response of output fields x_2 and x_1 while the input field y_2 is varied and y_1 is held constant. The thin red and thin green lines indicate stable steady states, while the dashed black line indicates unstable steady states which are physically inaccessible. The thick blue line indicates unstable steady states associated with instability. The parameters are $|y_1| = 0.5$, $C_1 = 200$, $C_2 = 2000$, $\gamma_1 = 1$, $\gamma_2 = 1$, $\nu = 0.1$, $\kappa_1 = 1$, $\kappa_2 = 1$, $\Delta_1 = 0$, $\Delta_2 = 0$, $\theta_1 = 0$, and $\theta_2 = 5$. All the frequency quantities are in units of γ_2^{-1}.

A. Λ system

The three-level Λ system in a double-cavity configuration is presented here. We fix the strength of one of the input fields, say y_1, coupling the atomic transition $|2\rangle \leftrightarrow |1\rangle$ to a constant value, and then vary the other input field, y_2 (which couples the adjacent atomic transition $|2\rangle \leftrightarrow |3\rangle$), to obtain the bistable response of y_2 versus x_2, as well as y_2 versus x_1, as shown in Fig. 2. The variation of the cavity output field x_1 due to the change in y_2 indicates the strong coupling and mutual dependence between the cavity fields x_1 and x_2 aided by the atom. We have undertaken the linear stability analysis about the fixed points (steady state) and identified the unstable regions in the lower branch (indicated as a thick blue line) as shown in Fig. 2. The usual unstable states associated with the negative slope of the *S*-shaped bistable response continue to exist (indicated as a dashed black line). The dynamical evolution of both fields occurs simultaneously and they mimic each other to a large extent. One can also obtain unstable states on the top branch by introducing finite cavity field detuning, akin to the instability obtained earlier [6,7]. We further analyze these unstable states through the bifurcation diagram and these can be associated with either periodic self-pulsing or chaotic dynamics (see Figs. 2 and 4). The stability of the periodic self-pulsing behavior is examined through the Floquet analysis, whereas the existence of the chaos is confirmed through the Lyapunov exponents (Ly) which take positive values corresponding to the chaotic regime [see Fig. 3(b)]. As we vary the input field y_2, the chaotic instability arises through a period doubling (PD) route, as shown in the inset of Fig. 3(a), wherein at least one of the Floquet multipliers (Fl) crosses out of the unit circle along the negative real axis [27]; specifically, for $|y_2| = 83.131$ the dominant Fl is 1, and for $|y_2| = 83.146$ the dominant Fl is -1.0025. In

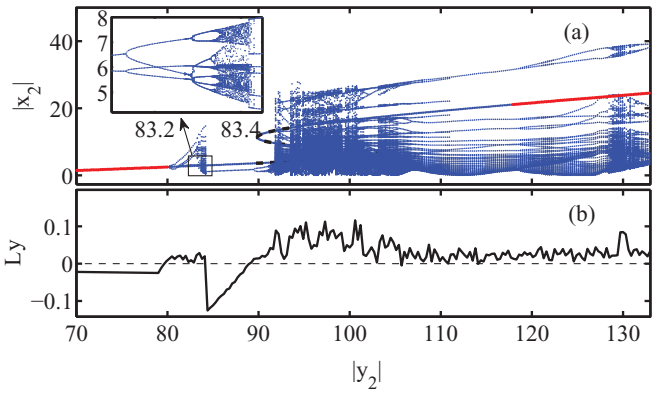

FIG. 3. (Color online) Λ system. (a) The bifurcation diagram corresponding to the AOB curve shown in Fig. 2(a), where the stable steady states and unstable steady states correspond to normal switching and self-pulsed or chaotic output, respectively. (b) The corresponding largest Lyapunov exponent. The parameters are the same as in Fig. 2.

order to obtain instability on the top branch, it is essential to have finite cavity detuning, and we have chosen $\theta_2 = 5$. In this regime, the output amplitude of the chaotic oscillation extends from the lower branch to the top branch of the AOB response. The coexistence of chaotic and normal stable solutions occurs for higher input field strengths. The temporal evolution and the frequency spectrum of the cavity output fields for two input field strengths (having two different $|y_2|$ values) corresponding to periodic self-pulsing and chaotic behavior are shown in Fig. 4. The presence of the double feedback plays a crucial role in creating these instabilities. This instability is suppressed if the feedback for one of the fields is removed. The competition between atom-field nonlinear interaction along the two cooperative branches and the associated decay pathways within the atom play a critical role in obtaining these instabilities, which are quite robust and occur over a wide parameter range. The parameter space associated with this system is extremely large, with 14 independent physical parameters involving decays, detunings, and couplings. In

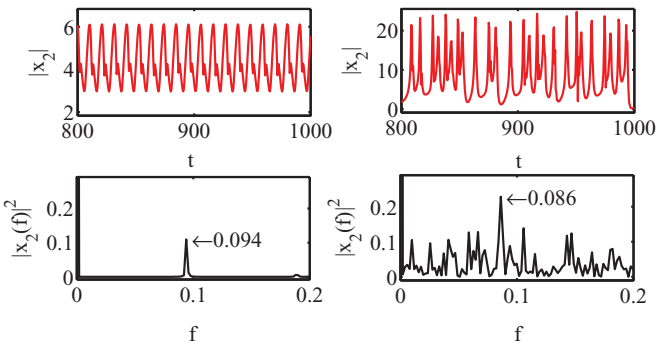

FIG. 4. (Color online) Λ system. Top: The temporal evolution indicating periodic self-pulsing and chaotic dynamics are shown in the left and right panels, respectively. Bottom: The associated frequency spectral density plots. The operating point $|y_2| = 83.1$ for periodic self-pulsing and $|y_2| = 95.2$ for chaotic behavior, and the other parameters are the same as in Fig. 2. Time t is in units of κ_2^{-1} and f is in units of κ_2.

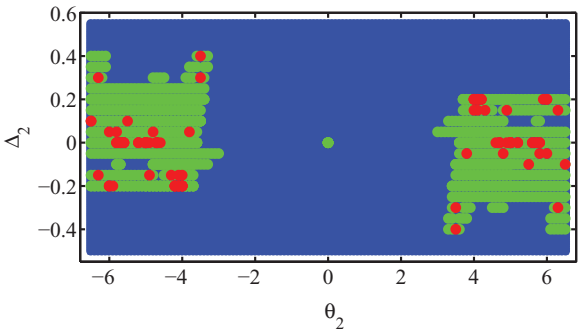

FIG. 5. (Color online) Λ system. Stability domain map indicating the stable-fixed-point region (blue), the self-pulsing region (green), and the chaotic region (red) as the atomic detuning (Δ_2) and the cavity detuning (θ_2) are varied. The other parameters are the same as given in Fig. 2 with $|y_1| = 0.5$ and $|y_2| = 91.9$.

order to steer the system systematically across the variety of instabilities, we take recourse to stability domain maps between two system parameters such as detunings θ_2 and Δ_2, which are shown in Fig. 5 with $|y_2| = 91.9$ corresponding to the lower (cooperative) branch of the AOB curve. One can identify islands of chaos (red) within the periodic self-pulsing domains (green), as well as regimes of normal switching (blue). Note that the instability in the cooperative branch exists even in the purely absorptive limit of atomic and cavity detunings ($\theta_2 = \Delta_2 = 0$), and it is very sensitive to the variation of detunings around the resonance point.

B. V system

We would like to explicitly bring out the importance of the incoherent (decay) pathways within the atom that are crucial to the occurrence of instability. The absorptive AOB relies on *collective absorption* in the *cooperative* (lower) branch, in contrast to a saturation of independent atoms in the one-atom (upper) AOB branch. Thus, the preparation of the *collective* state in the atomic ground state is crucial for realizing regular switching in AOB. The incoherent processes that directly affect this *collective* preparation of the atoms leads to instability, such as self-pulsing and chaos. A slow time scale can be associated with the decay of the initial preparation of the atom in the ground state, whereas a nonlinear interaction of the atoms and the fields within the cavity provides the fast time scale, and a competition between these time scales leads to the self-pulsing behavior. We note that in the Ξ and Λ configurations, the intermediate-state decay and the ground-state decoherence, respectively, provide the incoherent decay pathways that turn the state that is responsible for collective absorption *leaky*, leading to instability. However, in the V system, the shared ground state across the two transitions cannot be *leaky* and does not lead to any instability in the lower (cooperative) branch of the AOB. Essentially, it behaves like a pair of two-level atoms interacting independently with coherent cavity fields, coupled to a common ground state. Thus, in order to produce instability, we again address the *collective* state and introduce an incoherent pump between the ground state to one of the excited states [i.e., from $|3\rangle$ to $|1\rangle$, as shown in Fig. 1(b)]. The introduction of this incoherent pathway leads to unstable

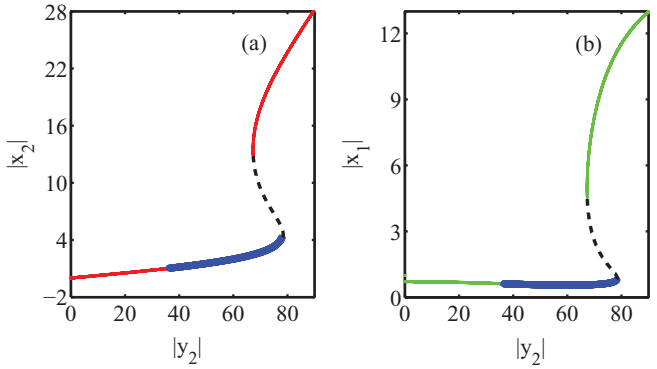

FIG. 6. (Color online) V system. (a), (b) Bistable response of output fields x_2 and x_1 while the input field y_2 is varied and y_1 is held constant. The thin red and thin green lines indicate stable steady states, while the dashed black line indicates unstable steady states which are physically inaccessible. The thick blue line indicates unstable steady states associated with instability. The parameters are $C_1 = 200, C_2 = 200, |y_1| = 15$, $\gamma_1 = 1, \gamma_2 = 1, \nu = 0.2, \kappa_1 = 1, \kappa_2 = 1, \Delta_1 = 0, \Delta_2 = 4.5, \theta_1 = 0, \theta_2 = -2.5$, and $r = 2$. All of the frequency quantities are in units of γ_2^{-1}.

steady states over the lower branch of the AOB curve, shown in Fig. 6 (indicated with a thick blue line), and is essential for obtaining optical instability. The associated bifurcation diagram is given in Fig. 7, and again indicates the transition of the cavity output field from normal stable switching to chaos through a period doubling route, as shown in the inset. We also determined the Lyapunov exponents [see Fig. 7(b)] to demarcate the range of input field $|y_2|$ which lead to these instabilities.

In general, with variation in the system parameter ($|y_2|$ in the present case), the nonlinear dynamical self-pulsing behavior is expected to occur beyond the Hopf (H) bifurcation point that separates the normal switching from periodic self-pulsing. Interestingly periodic self-pulsing behavior coexists with stable switching for a range of $|y_2|$ (see region around $|y_2| = 37$ shown in Fig. 7). To understand such coexistence, we use the limit-cycle continuation from the Hopf point using

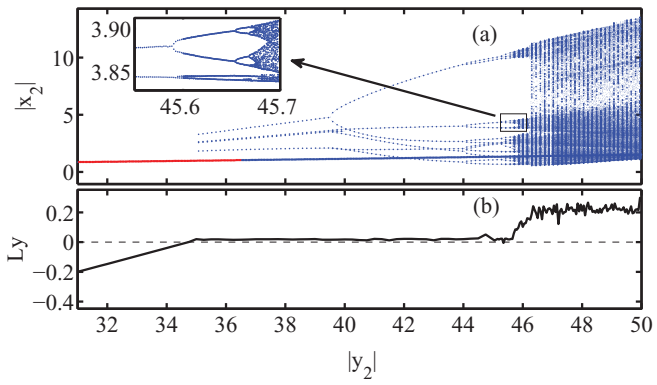

FIG. 7. (Color online) V system. (a) The bifurcation diagram corresponding to the lower branch of the AOB curve shown in Fig. 6(a), where the stable steady states and unstable steady states correspond to normal switching and self-pulsed or chaotic output, respectively. (b) The corresponding largest Lyapunov exponent. The parameters are the same as in Fig. 6.

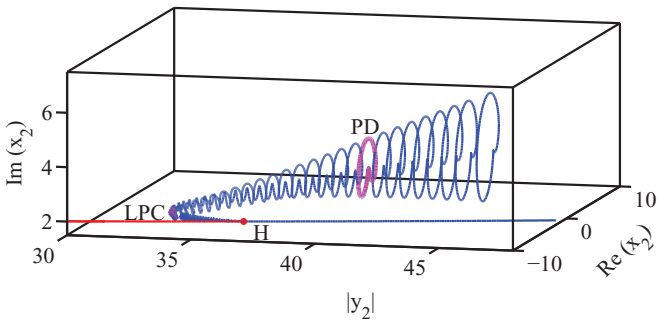

FIG. 8. (Color online) V system. The limit cycle continuation from the Hopf (H) point at the very onset of instability on the lower branch of the AOB curve shown in Fig. 6(a). The limit point of cycles (LPC) as well as the period doubling (PD) point are indicated as thick magenta loops. The parameters are the same as in Fig. 6.

the MATCONT continuation package [28]. The continuation diagram is shown in Fig. 8 and indicates that the limit-cycle continuation initially occurs in the direction of decreasing $|y_2|$ up to $|y_2| = 35$, and then turns around at a limit point of cycles (LPC); this is also known as the fold bifurcation point (indicated in magenta).

The dominant Floquet multipliers plotted on the complex plane indicate that the periodic self-pulsing behaviors (limit cycles) associated with continuation in the increasing and decreasing variation of $|y_2|$ are stable and unstable, respectively. Therefore, all three possible behaviors (normal switching and stable and unstable periodic self-pulsing) coexist in the lower AOB branch region within the interval $|y_2| = [35,36]$. Hence, depending on the initial condition, the appropriate behavior will be observed. The period doubling route described in the above bifurcation diagram is also corroborated by the presence of the period doubling (PD) cycle indicated as a magenta loop in Fig. 8. Such bifurcation phenomena could be promising for the appearance of oscillating cavity solitons in a V system, once diffraction is included in the model equations [29,30]. However, we do not invoke any transverse field dependence for obtaining the instabilities. The connection between the two seems potentially rich and needs to be explored.

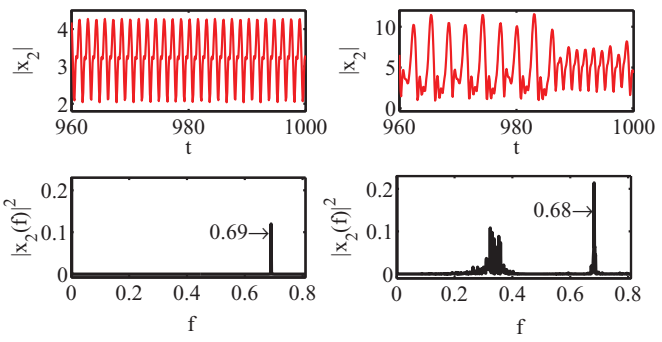

FIG. 9. (Color online) V system. Top: The temporal evolution of periodic self-pulsing and chaotic dynamics are shown in the left and right panels, respectively. Bottom: The associated frequency spectral density plots. The operating point $|y_2| = 38$ for periodic self-pulsing and $|y_2| = 47$ for chaotic behavior, and the other parameters are the same as in Fig. 6. Time t is in units of κ_2^{-1} and f is in units of κ_2.

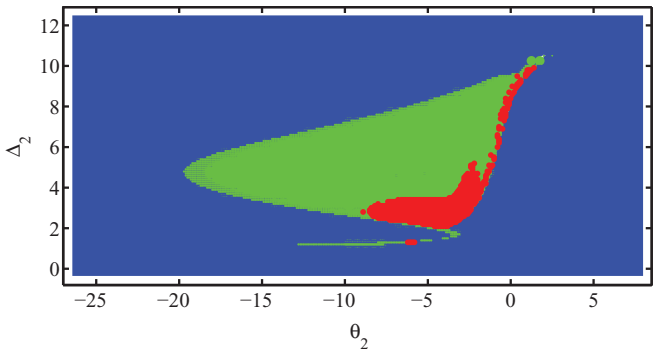

FIG. 10. (Color online) V system. Stability domain map indicating the stable-fixed-point region (blue), the self-pulsing region (green), and the chaotic region (red) as the atomic detuning (Δ_2) and the cavity detuning (θ_2) are varied. The other parameters are the same as given in Fig. 6 with $|y_1| = 15$ and $|y_2| = 50$.

In Fig. 9, we present the temporal evolution of the cavity output field corresponding to stable periodic self-pulsing and chaotic operating regimes, and the corresponding frequency spectrum in the bottom panels. The domain map plotted between the detunings θ_2 and Δ_2 (see Fig. 10) portrays the various regions such as normal switching (blue), periodic self-pulsing (green), and chaotic behavior (red) associated with cavity output. Before we conclude, we indicate the possible experimental system, where these effects can be realized, using rubidium (^{87}Rb, D_1 line) atomic vapor in the Λ- and V-type configuration along the transitions $5S_{1/2}(F = 2) \leftrightarrow 5P_{1/2}(F' = 2) \leftrightarrow 5S_{1/2}(F = 1)$ and $5P_{3/2} \leftrightarrow 5S_{1/2} \leftrightarrow 5P_{1/2}$, respectively. Considering temperatures of about 60 °C, one would obtain a number density of $\approx 10^{11}$ atoms/cm^3 and, with transmission coefficient $T_i \approx 10^{-2}$, it would result in cooperative parameter $C_i \approx 1000$. The input power levels can be varied from ≈0–20 mW across a spot size of 100 μm to observe effects we have mentioned in this paper. The different values of cooperative parameter can be realized by changing either the number density of atoms or the transmission coefficient of the cavity. The range of parameters is explicitly enumerated in Table I. The $4D_{3/2} \leftrightarrow 5P_{3/2} \leftrightarrow 4D_{5/2}$ transitions in ^{87}Rb offer promising implementation of these effects in the optical communication wavelength range of 1.5 μm with degenerate fields [31].

TABLE I. Parameters and their range. All of the frequency parameters are scaled with $\gamma_2 = 36$ MHz.

Parameters	Symbol	Range
Atomic detuning	$\Delta_{1,2}$	$-10 \leftrightarrow 10$
Cavity decays	$\kappa_{1,2}$	$0 \leftrightarrow 1$
Cavity detuning	$\theta_{1,2}$	$-10 \leftrightarrow 10$
Cooperative parameters	$C_{1,2}$	$100 \leftrightarrow 1000$
Input field strengths	$\lvert y_{1,2}\rvert$	$0 \leftrightarrow 150$
Nonradiative decay	ν	$0 \leftrightarrow 1$
Incoherent pumping rate	r	$0 \leftrightarrow 1$

IV. CONCLUSION AND REMARKS

We have demonstrated methods of generating periodic self-pulsing and chaotic instability using a double-cavity AOB system having a three-level atomic medium in the Λ and V configurations. These instabilities occur in the lower branch of the bistable curve and are intrinsically related to the competition of cooperative behavior of the atomic collection along the two adjacent transitions as well as the details of the incoherent pathways within the atom. The ground-state decoherence is sufficient for the Λ system to exhibit instability; however, by introducing an appropriate incoherent pathway (incoherent pump), we induce instability even in the V-system double-cavity AOB. Hence, the incoherent pathway needs to deplete the collection of atoms involved in the cooperative effect to exhibit instabilities. All of the instabilities are obtained under the mean-field approximation.

ACKNOWLEDGMENT

We gratefully acknowledge Dr. Pankaj Wahi for discussions related to nonlinear dynamical aspects of this work.

[1] Guido H. M. van Tartwijk and Govind P. Agrawal, Prog. Quantum Electron. **22**, 43 (1998).
[2] H. Haken, in *Handbuch der Physik, Light and Matter*, edited by L. Genzel (Springer-Verlag, Berlin, 1970), Vol. 25/2c.
[3] H. Haken, Z. Phys. **190**, 327 (1966).
[4] G. Khitrova, J. F. Valley, and H. M. Gibbs, Phys. Rev. Lett. **60**, 1126 (1988).
[5] *Instabilities and Chaos in Quantum Optics* (Springer Series in Synergetics), edited by Arecchi F. Tito and Robert G. Harrison (Springer-Verlag, Berlin, 1987), Vol. 34.
[6] L. A. Lugiato, L. M. Narducci, D. K. Bandy, and C. A. Pennise, Optics Commun. **43**, 281 (1982).
[7] L. A. Orozco, and H. J. Kimble, A. T. Rosenberger, L. A. Lugiato, M. L. Asquini, and M. Brambilla, L. M. Narducci, Phys. Rev. A **39**, 1235 (1989).
[8] B. Segard, B. Macke, L. A. Lugiato, F. Prati, and M. Brambilla, Phys. Rev. A **39**, 703 (1989).
[9] H. A. Babu and Harshawardhan Wanare, Phys. Rev. A **83**, 033818 (2011).
[10] H. A. Babu and Harshawardhan Wanare, Phys. Rev. A **83**, 033819 (2011).
[11] Wenge Yang, Amitabh Joshi, and Min Xiao, Phys. Rev. Lett. **95**, 093902 (2005).
[12] K. I. Osman and A. Joshi, Phys. Lett. A **376**, 2565 (2012).
[13] M. A. Anton and Oscar G. Calderon, J. Opt. B: Quantum Semiclassical Opt. **4**, 91 (2002).
[14] A. Joshi, W. Yang, and M. Xiao, Phys. Rev. A **68**, 015806 (2003).
[15] D. F. Walls and P. Zoller, Opt. Commun. **34**, 260 (1980).
[16] D. F. Walls, P. Zoller, and M. L. Steyn-Ross, IEEE J. Quantum Electron. **17**, 380 (1981).

[17] G. D. VanWiggeren and Rajarshi Roy, Science **279**, 1198 (1998).
[18] A. Uchida, J. Garcia-Ojalvo, F. Rogister and Rajarshi Roy, in *Progress in Optics*, edited by E. Wolf (North-Holland, Amsterdam, 2005), Vol. 48, p. 203.
[19] L. A. Lugiato, in *Progress in Optics*, edited by E. Wolf (North-Holland, Amsterdam, 1984), Vol. XXI, p. 69.
[20] J. Gea-Banacloche, Y. Q. Li, S. Z. Jin, and M. Xiao, Phys. Rev. A **51**, 576 (1995).
[21] M. Fleischhauer, C. H. Keitel and M. O. Scully, Chang Su, B. T. Ulrich, and Shi-Yao Zhu, Phys. Rev. A **46**, 1468 (1992).
[22] L. M. Narducci, W. W. Eidson, P. Furcinitti, and D. C. Eteson, Phys. Rev. A **16**, 1665 (1977).
[23] P. Galatola, L. A. Lugiato, M. Vadacchino, and N. B. Abraham, Opt. Commun. **69**, 414 (1989).
[24] G. P. Agrawal and C. Flytzanis, Phys. Rev. Lett. **44**, 1058 (1980).
[25] G. P. Agrawal and C. Flytzanis, Phys. Rev. A **24**, 3173 (1981).
[26] H. A. Babu and Harshawardhan Wanare, Phys. Rev. A **87**, 033821 (2013).
[27] Steven H. Strogatz, *Nonlinear Dynamics and Chaos* (Perseus, New York, 1994).
[28] A. Dhooge, W. Govaerts, and Yu. A. Kuznetsov, ACM Trans. Math. Software **29**, 141 (2003). MATCONT package is available at http://www.matcont.ugent.be.
[29] L. A. Lugiato and R. Lefever, Phys. Rev. Lett **58**, 2209 (1987).
[30] Germán J. de Valcárcel and Kestutis Staliunas, Phys. Rev. A **87**, 043802 (2013).
[31] Han Seb Moon, Lim Lee, and Jung Bog Kim, J. Opt. Soc. Am. B **24**, 2157 (2007).